CHINESE OPTICS LETTERS

Vol. 21, No. 7 | July 2023

Intrapulse coherence degradation suppressing method of echo signal in coherent lidar

Haisheng Cong (从海胜)[1,2], Jianfeng Sun (孙建锋)[3*], Zhiyong Lu (卢智勇)[1], Hongyu He (贺红雨)[1], Weijie Ren (任伟杰)[1,2], Yuxin Jiang (姜玉鑫)[1,2], Lingling Xu (许玲玲)[1,2], Chaoyang Li (李超洋)[1], Longkun Zhang (张龙坤)[1], and Zhengwei Zhang (张正伟)[1]

[1] Key Laboratory of Space Laser Communication and Detection Technology, Shanghai Institute of Optics and Fine Mechanics, Chinese Academy of Sciences, Shanghai 201800, China

[2] Center of Materials Science and Optoelectronics Engineering, University of Chinese Academy of Sciences, Beijing 100049, China

[3] Department of Aerospace Laser Engineering, Shanghai Institute of Optics and Fine Mechanics, Chinese Academy of Sciences, Shanghai 201800, China

*Corresponding author: sunjianfengs@163.com

Received December 13, 2022 | Accepted April 18, 2023 | Posted Online July 25, 2023

Aiming at coherence degradation during target detection, a suppressing method based on frequency-modulated continuous wave coherent lidar is proposed. Combined with a random iteration algorithm, a long-pulse echo signal with coherent degradation is matched with random phase noise of a certain frequency and achieves coherence restoration. Simulation and field experiment results show that this proposed method can recover the intrapulse coherence in long-pulse echo signals. In addition, for the real target echo signal at 4.2 and 19.8 km, the peak signal-to-noise ratio processed by this method is increased by 0.35 times and 4 times after pulse compression, respectively.

Keywords: coherent lidar; long-pulse signal; coherent degradation; frequency modulation continuous wave.
DOI: 10.3788/COL202321.071201

1. Introduction

Compared with traditional radar, light detection and ranging (lidar) has several advantages and is widely applied in several areas, such as automatic driving, artificial intelligence, and drone reconnaissance[1–4]. However, during the target detection, some factors such as laser resource coherence length, atmosphere turbulence, and target scattering characteristics, have a serious influence on the performance of lidar, which can easily lead to phase disturbance in long-pulse echo signals and severely restrict the performance of the lidar[5–9].

The ranging accuracy of the femtosecond pulse lidar depends on the pulse width of the echo beam after propagating over a long path. In addition, the temporal dispersion easily caused by optical components, atmosphere, or seawater factors during its propagation results in intrapulse coherence degradation and pulse widening of the echo signal, which decreases the ranging accuracy of the lidar[10–13]. For this problem, Lee *et al.* compensated for the dispersion effect by combining single-mode fiber with actively controlled prism pairs to improve the detection accuracy of pulse lidar[11]. Fan *et al.* applied the speckle noise reduction technique based on self-adaptive pulse matching independent component analysis to suppress speckle noise[14]. However, the threshold selection of the wavelet threshold algorithm may distort the effective signal. Similarly, these factors, such as atmospheric turbulence, dispersion, target characteristics, and vibration, could cause phase disturbance in long-pulse echo signals to broaden the signal spectral width, reducing the peak signal-to-noise ratio (SNR) of the echo signal, and limiting the resolution and accuracy for coherent lidar[9,15–18]. Zheng *et al.* adopted a dual-frequency laser seed source to eliminate the signal coherence degradation effect caused by atmospheric turbulence and improve the peak SNR of the intermediate signal[19]. However, it is necessary to make the wavelengths of the two lasers as close as possible to ensure the correlation of the effects of atmospheric disturbance on dual-frequency lasers. Zhao *et al.* adopted the frequency sampling method to correct the nonlinear effect of the frequency-modulated continuous wave (FMCW) laser source and analyzed the influence of fiber dispersion on the velocity measurement and ranging in coherent lidar[20]. Wang *et al.* constructed a T-FMCW particle filter to compensate for temporal vibration errors and residual nonlinear errors[21].

For the FMCW coherent lidar, the nonlinear modulation effect can also lead to decoherence and spectrum broadening of the echo signal, which also limits the ranging performance of the lidar. Dilazaro, Yang, and Zhang *et al.*, respectively, used a photoelectric phase-locked loop, back propagation neural networks combined with proportion-integration-differentiation

control, iterative learning predistortion, and other methods to reduce laser phase noise and sweep error[22–24]. All the above schemes need to set feedback loops around the FMCW laser source, which undoubtedly increases the complexity of the system. Based on the dynamic range measurement method of dual lasers, Yu *et al.* adopted the frequency modulation nonlinear kernel function to reduce the dispersion mismatch influence, thus improving the ranging and velocity measurement accuracy in FMCW[25]. But the calibration accuracy of the method depends on the phase accuracy of the signal obtained by the auxiliary interferometer, which may be influenced by external factors. Meanwhile, Bai *et al.* adopted a nonlinear correction method based on singular value decomposition and least squares algorithm to improve the SNR of long-pulse echo signals by minimizing the phase error between the fitted phase and the true phase and accurately calculating the nonlinear coefficients of each order[26]. The method has a high demand for sampling points and needs to select a reasonable number of sampling points.

Different from the above methods, this paper directly proposes a coherence degradation suppression method for long-pulse echo signals with coherence degradation. Compared with the above schemes, the intrapulse coherence degradation suppressing method proposed in this paper does not require additional feedback circuits, and it does not have a high demand for sampling points. Meanwhile, the proposed method processes phase errors directly without the phase mechanism and model construction. Based on FMCW coherent lidar, the influence of random phase disturbance on the peak SNR of the long-pulse echo signal is analyzed in detail from a theoretical point view, and then the intrapulse coherent degradation suppressing method in long-pulse echo signal is verified through numerical simulation and field experiment. The results show that this proposed method can effectively suppress the intrapulse coherence degradation in long-pulse echo signals, improve the pulse compression peak SNR, and further enhance the detection capability of coherent lidar. It is important for the application of coherent lidar in remote target detection, the limited laser coherence length, and phase disturbance.

2. Analysis of Coherence Degradation Effects

It is assumed that the pulse repetition rate in T-FMCW is PRF, modulation bandwidth is B, and pulse half-period T is equal to $1/(2 \cdot \mathrm{PRF})$ as shown in Fig. 1, so the emitted light field expression is

$$u_T(t) = E_T \exp[-j(2\pi f_0 t + \pi k t^2) + j\varphi_{T0}], \quad (1)$$

where E_T is the amplitude of emitted light; f_0 is laser carrier frequency; k is the chirp rate; and φ_{T0} is the initial phase of emitted light. Meanwhile, the local oscillator light-field expression is

$$u_{\mathrm{LO}}(t) = E_{\mathrm{LO}} \exp[-j(2\pi f_0 t + \pi k t^2) + j\varphi_{\mathrm{LO0}}], \quad (2)$$

where E_{LO} is the amplitude of the local oscillator light field, and φ_{LO0} is the initial phase of the local oscillator light field.

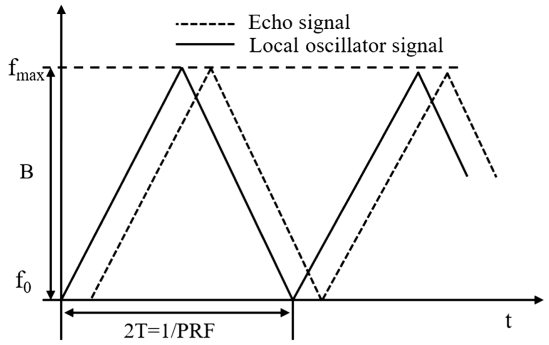

Fig. 1. Relationship between frequency and time in T-FMCW.

For a stationary target at L (in km), the optical field expression $u_S(t)$ of the echo signal is

$$u_S(t) = E_S \exp\{-j[2\pi f_0(t-\tau) + \pi k(t-\tau)^2]\} \exp(-j\varphi_{S0}), \quad (3)$$

where E_S is the amplitude of the echo signal; τ represents the time delay and is equal to $2L/c$; c is light speed; and φ_{S0} is the initial phase of the echo signal.

For coherent lidar with I/Q receivers as shown in Fig. 2, I and Q channel echo signals (ignoring the part of the second-order phase), respectively, are

$$\begin{aligned} x_I(t) &= s_I(t) + n_I(t) \\ &= G\beta E_{\mathrm{LO}} E_S \cos(2\pi f_0 \tau + 2\pi k\tau t - \pi k\tau^2 + \Delta\varphi_I) + n_I(t), \end{aligned} \quad (4)$$

$$\begin{aligned} x_Q(t) &= s_Q(t) + n_Q(t) \\ &= G\beta E_{\mathrm{LO}} E_S \sin(2\pi f_0 \tau + 2\pi k\tau t - \pi k\tau^2 + \Delta\varphi_Q) + n_Q(t), \end{aligned} \quad (5)$$

where $s_I(t)$ and $s_Q(t)$ represent the effective signal in the I/Q channel; $n_I(t)$ and $n_Q(t)$ represent band-limited Gaussian white noise (GWN), which meets the same statistical distribution of parameters in both balanced photodetectors of the I/Q channel. For the sake of analysis, it is assumed that the effective bandwidth of GWN is B_n, and GWN satisfies the Gaussian distribution whose mean value is 0 and the variance is σ_n^2; σ_n^2 is constant; G is the photodetector gain; β is the photodetector responsivity and is equal to $\eta_D e/hf_0$, where η_D is the quantum efficiency; e is the electron charge constant; h is the Planck constant; $\Delta\varphi_I$ is the phase difference between echo signal phase $\Delta\varphi_{S0}^I$ and local signal phase $\Delta\varphi_{\mathrm{LO0}}^I$ in I channel; and $\Delta\varphi_Q$ is the phase difference

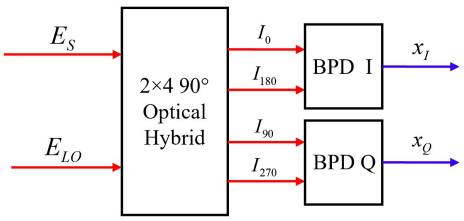

BPD: Balanced photodetector

Fig. 2. Block diagram with I/Q receiver.

between the echo signal phase $\Delta\varphi_{S0}^{Q}$ and the local signal phase $\Delta\varphi_{LO0}^{Q}$ in the Q channel.

For the convenience of analysis, the complex echo signal of coherent lidar is[27]

$$\begin{aligned} x(t) &= x_I(t) + jx_Q(t) \\ &= G\beta E_{LO}E_S \exp(j2\pi f_0\tau + j2\pi k\tau t - j\pi k\tau^2 + j\Delta\phi) \\ &\quad + E_N(t)\exp[j\phi_N(t)], \end{aligned} \tag{6}$$

where $\Delta\phi$ is the phase difference, assuming that $\Delta\phi$, $\Delta\varphi_I$, and $\Delta\varphi_Q$ are the same; $E_N(t)$ is the random noise amplitude; and $\phi_N(t)$ is the random noise phase.

Combined with pulse compression, a long-pulse echo signal with a low chirp rate could be compressed into a narrow pulse with high peak intensity, which largely improves the detection sensitivity of lidar[28]. The long-pulse period echo signal after pulse compression ($\tau \ll T$) is

$$X(f) = G\beta E_{LO}E_S \cdot T\,\mathrm{sinc}[\pi T(f - f_r)]\exp(j\varphi) + N(f), \tag{7}$$

where sinc(·) is the sinc function; f_r is the intermediate frequency (IF) of the echo signal and is equal to $k\tau$; φ is a constant phase in long-pulse echo signal and is equal to $2\pi f_0\tau - \pi k\tau^2 + \Delta\phi$; and $N(f)$ represents the random noise spectrum distribution. Accordingly, the power spectrum density (PSD) of the long-pulse echo signal is

$$P(f) = G^2\beta^2 P_S P_{LO} \cdot T\,\mathrm{sinc}^2[\pi T(f - f_r)] + \sigma_n^2/B_n, \tag{8}$$

where P_{LO}, P_S represent respectively local oscillator signal optical power and echo signal optical power, which, respectively, correspond to E_{LO}^2 and E_S^2.

In addition, band-limited GWN mainly depends on shot noise in heterodyne detection, so the random noise variance σ_n^2 is $G^2\beta eB_nP_{LO}$. Finally, the peak SNR of long-pulse echo signal without coherence degradation is

$$\mathrm{SNR} = \frac{G^2\beta^2 P_{LO}P_S T \cdot \Delta f}{(\sigma_n^2/B_n)\cdot\Delta f} = \frac{\eta_D P_S T}{hf_0}, \tag{9}$$

where Δf represents frequency resolution and is equal to $1/T$.

In general, a long-pulse echo signal can attain more accumulation time compared with a short-pulse echo signal in coherent lidar. However, in practice, phase fluctuation deteriorates the intrapulse coherence of the long-pulse echo signal. Ultimately, it can decrease effective accumulation time after pulse compression and affects the target detection capability of coherent lidar[6].

To simplify the analysis, assuming that random phase perturbation $\varphi_{add}(t)$ is a stationary stochastic process, a long-pulse echo signal $x'(t)$ with intrapulse coherence degradation is

$$\begin{aligned} x'(t) &= G\beta E_{LO}E_S \exp(j2\pi k\tau t + j\varphi)\exp[j\varphi_{add}(t)] \\ &\quad + E_N(t)\exp[j\phi_N(t)]. \end{aligned} \tag{10}$$

Assuming that the long-pulse echo signal is independent of GWN, the autocorrelation function of the long-pulse echo signal $x'(t)$ is

$$\begin{aligned} R(\tau') &= \langle x'^*(t)x'(t+\tau')\rangle \\ &= \langle (G\beta E_{LO}E_S)^2 \exp(j2\pi k\tau\tau')\cdot\exp[j\Delta\varphi_{add}(t,\tau')]\rangle \\ &\quad + \langle E_N(t)E_N(t+\tau')\exp\{j[\phi_N(t+\tau') - \phi_N(t)]\}\rangle, \end{aligned} \tag{11}$$

where $\Delta\varphi_{add}(t,\tau')$ represents the phase difference between $\varphi_{add}(t+\tau')$ and $\varphi_{add}(t)$. Combined with the statistical characteristics of random phase disturbance, it is known that $\Delta\varphi_{add}(t,\tau')$ is a stationary random Gaussian process whose mean is zero and whose distribution function is

$$f[\Delta\varphi_{add}(\tau')] = \frac{1}{[2\pi\langle\Delta\varphi_{add}^2(\tau')\rangle]^{1/2}}\cdot\exp\left[-\frac{\Delta\varphi_{add}^2(\tau')}{2\langle\Delta\varphi_{add}^2(\tau')\rangle}\right], \tag{12}$$

where $\langle\Delta\varphi_{add}^2(\tau')\rangle$ represents mean square value and is equal to $2\pi^2 n_0|\tau'|$, where n_0 is the PSD of $\Delta\varphi_{add}(t,\tau')$, so $\langle\exp[j\Delta\varphi_{add}(t,\tau')]\rangle$ in $R(\tau')$ is equal to $\exp[-\langle\Delta\varphi_{add}^2(\tau')\rangle/2]$.

The autocorrelation function of long-pulse echo signal $x'(t)$ with intrapulse coherence degradation is simplified as[29]

$$\begin{aligned} R(\tau') &= (G\beta E_{LO}E_S)^2\exp(-2\pi^2 n_0|\tau'|)\exp(j2\pi k\tau\tau') \\ &\quad + \sigma_n^2\frac{\sin(\pi B_n\tau')}{\pi B_n\tau'}. \end{aligned} \tag{13}$$

According to the Wiener–Khinchin theorem, the PSD function of a long-pulse echo signal $x'(t)$ is

$$\begin{aligned} P'(f) &= G^2\beta^2 P_{LO}P_S \cdot T\,\mathrm{sinc}[\pi T(f - f_r)] \\ &\quad * \frac{n_0}{f^2 + (\pi n_0/2)^2} + \frac{\sigma_n^2}{B_n}, \end{aligned} \tag{14}$$

where $A*B$ is the convolution operation between A and B. Defining $Y(T,f)$ as the partial differential of the PSD function $P'(f)$ to T, $Y(T,f)$ is

$$Y(T,f) = G^2\beta^2 P_{LO}P_S\cos[\pi T(f - f_r)] * \frac{n_0}{f^2 + (\pi n_0/2)^2}. \tag{15}$$

Therefore, this PSD function $P'(f)$ is analyzed in the following two cases.

(1) When T tends to infinity, $Y(T,f)$ is

$$Y(T,f) = \frac{G^2\beta^2 P_{LO}P_S n_0}{(f - f_r)^2 + (\pi n_0/2)^2}. \tag{16}$$

When f is equal to f_r, the peak SNR of the long-pulse echo signal after intrapulse coherence degradation is

$$\mathrm{SNR}' = \frac{\eta_D P_S T}{hf_0}\frac{4}{\pi^2 n_0} < \frac{\eta_D P_S T}{hf_0}. \tag{17}$$

(2) When T tends to be infinitesimal or f is extremely close to f_r, $Y(T,f)$ is

$$Y(T,f) = G^2\beta^2 P_{\mathrm{LO}} P_S \left[1 - \frac{1}{2}\pi^2 T^2 (f - f_r)^2\right] * \frac{n_0}{f^2 + (\pi n_0/2)^2}. \tag{18}$$

Based on the above, the value of $Y(T,f)$ gradually decreases as T increases. Especially, when f is equal to f_r, the peak SNR of the long-pulse echo signal after intrapulse coherence degradation is

$$\mathrm{SNR}' \le \frac{\eta_D P_S T}{h f_0}. \tag{19}$$

To more clearly analyze the influence of random phase disturbance on the long-pulse echo signal, it is necessary to define the peak SNR loss ratio γ,

$$\gamma = \frac{\mathrm{SNR} - \mathrm{SNR}'}{\mathrm{SNR}}. \tag{20}$$

Combined with theoretical analysis, it is known that the peak SNR loss ratio γ is less than 1 forever. It shows that intrapulse random phase disturbance can induce coherence degradation of the echo signal, resulting in energy dispersion and peak intensity decrease.

3. Suppressing Method of Coherence Degradation

As for this problem, the coherence degradation suppression method for long-pulse echo signals with coherent degradation is proposed in this paper, as shown in Fig. 3.

The working process of the proposed method is as follows.

First, attain the long-pulse echo signal with coherence degradation and select the amplitude as the initial amplitude from its frequency spectrum. Second, divide the long-pulse echo signal into N segments. Third, generate an N-segment random phase so that each segment random phase satisfies the Gaussian distribution. Then compensate for the N-segment echo signal with the N-segment random phase noise. Meanwhile, the number of iterations increases one by one, and the compensated echo signal performs a pulse compression after signal splicing. Next, reattain the frequency amplitude as the updated amplitude at the selected frequency point and compare the updated amplitude with the initial amplitude.

If the updated amplitude is not smaller than the initial amplitude, perform a random phase accumulation and then use it as the current phase, exchanging the updated amplitude with the initial amplitude. Subsequently, regenerate the N-segment random phase and sum the current phase with the N-segment random phase to compensate for the N-segment echo signal with the current phase.

If the updated amplitude is smaller than the initial amplitude, regenerate the N-segment random phase directly and sum the current phase with the N-segment random phase to compensate for the N-segment echo signal with the N-segment echo signal.

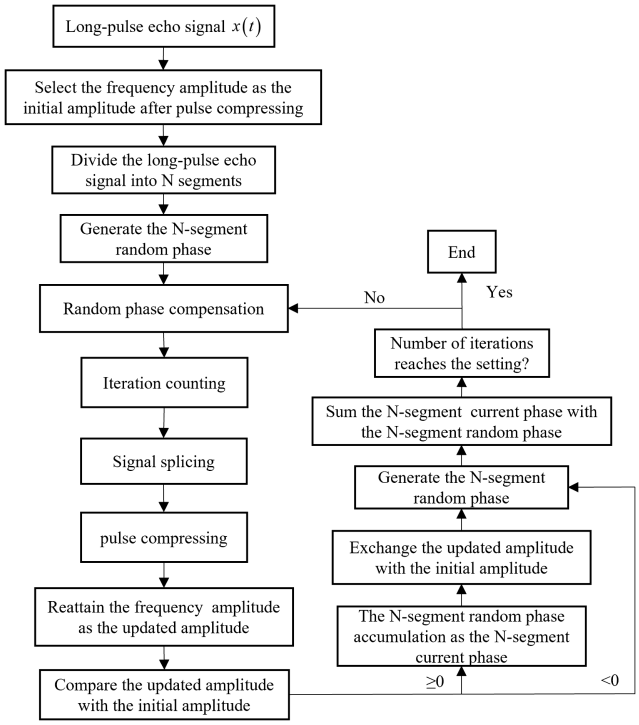

Fig. 3. Workflow of the proposed method.

Just like the workflow in Fig. 3, when the method finally converges, the current phase is regarded as the final compensating phase, and the echo signal could achieve coherence restoration after being compensated with it at this moment.

To attain the results at different random phase frequencies or different frequency points, it is necessary to change the segment number and frequency point, respectively.

To verify this method, a numerical simulation of the long-pulse echo signal in coherent lidar is performed with the parameters shown in Table 1.

Under the condition of random phase disturbance, a long-pulse echo signal with intrapulse coherence degradation is

Table 1. Parameters of Simulation.

Number	Parameter	Value
1	Pulse period	4 ms
2	Intermediate frequency	2 MHz
3	Sampling rate	20 MHz
4	SNR0 (with phase noise)	~25 dB
5	Random noise PSD	5 μW/Hz
6	Random frequency noise PSD	10×10^3 Hz^2/Hz
7	Random phase-matching frequency	250 Hz–50 kHz
8	Number of iterations	2000 times

processed by the method proposed in this paper, and the results shown in Fig. 4(a) are obtained. It shows that the frequency amplitude of long-pulse echo signal with coherent degradation rapidly increases at first and then tends to converge with the increase of the iteration number processed in this method. When the random phase-matching frequency is 25 kHz and the number of iterations is 1000, the frequency amplitude of the long-pulse echo signal with 4 ms is about 1.73 times higher compared with the echo signal after coherence degradation.

In addition, it can be seen that the frequency spectral width of the long-pulse echo signal with coherent degradation suppression after pulse compression is decreased by about 2 times in Fig. 4(b), which indicates that the method proposed in this paper can effectively suppress the intrapulse coherence degradation of the long-pulse echo signal.

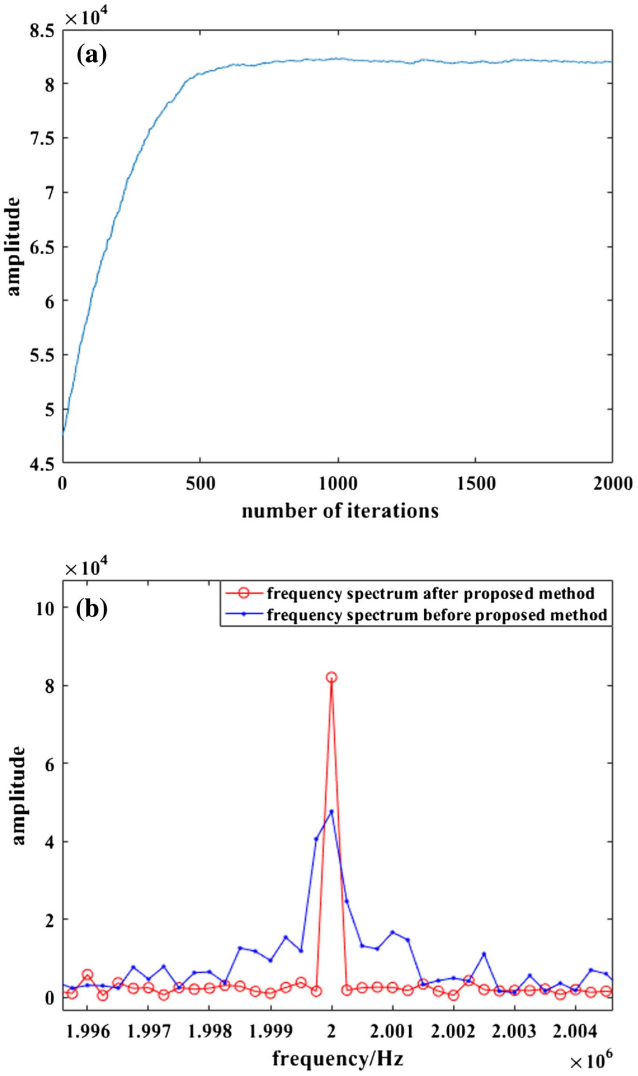

Fig. 4. Processing results of the proposed method. (a) Iterative process of the frequency peak intensity of long-pulse echo signal; (b) frequency spectrum of the long-pulse echo signal with coherent degradation comparison before and after the proposed method.

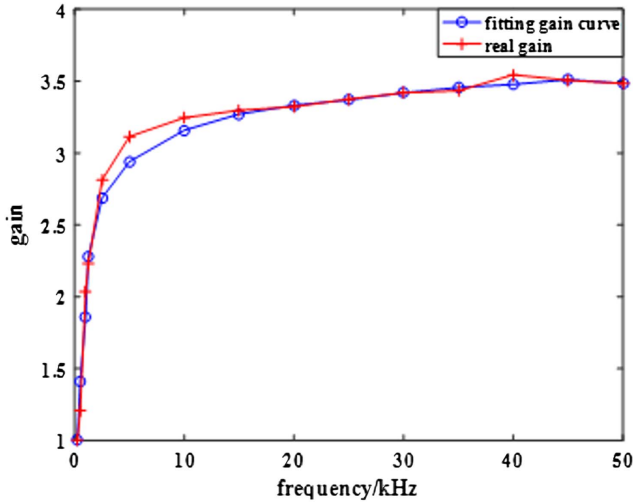

Fig. 5. Results of intrapulse coherence degradation suppression method for long-pulse echo signal with different random phase matching frequencies.

According to the random phase-matching frequency shown in Table 1, the long-pulse echo signals with coherence degradation are processed by the coherence degradation suppression method proposed in this paper, and the results shown in Fig. 5 are obtained. When the matching frequency of random phase disturbance is greater than 30 kHz, the peak SNR gain of the long-pulse echo signal with coherence degradation is maintained at 3.4 times. In the subsequent processing, the SNR gain of the long-pulse echo signal with pulse compression tends to be saturated as the matching frequency of random phase disturbance increases. In this case, the intrapulse coherence of the long-pulse echo signal is mostly restored.

4. Experimental Result and Analysis

To further verify the above method of suppressing the long-pulse echo signal with coherence degradation, a verification experiment was designed. As shown in Fig. 6, the FMCW laser source is split into an emitted signal and a local signal through a 1×2 fiber coupler. After the power amplification of the optical fiber amplifier, the emitted signal enters into free space through the optical transceiver and directly illuminates the static target. After the static target scattering, the echo signal light is transmitted again through free space and is received by the optical transceiver of the coherent lidar. Then, the echo signal light passes through the fiber circulator and performs a heterodyne detection with a local oscillator signal in the optical hybrid. The obtained beat optical signal is converted by a photodetector into an IF electrical signal, which is finally collected by a digital acquisition device.

Based on the above field verification experiment scheme, the FMCW parameter settings, optical transceiver telescope, and emitted beam power are shown in Table 2. In this field test, the visible light camera uses Nikon AF-S DX NIKKOR optical lens, and the type of charge-coupled device (CCD)

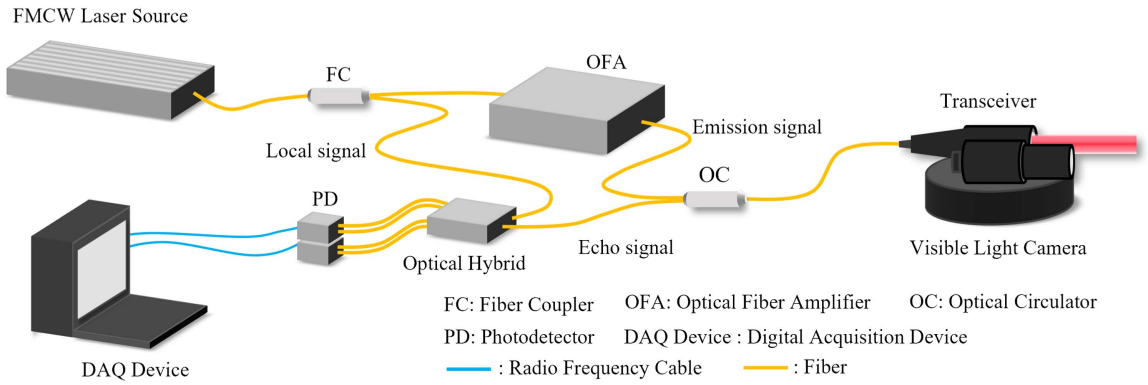

Fig. 6. Field verification experiment scheme.

Table 2. Experimental Parameters.

Number	Parameter	Value
1	PRF	250 Hz
2	Modulation bandwidth	300 MHz
3	Telescope diameter	50 mm
4	Transmission power	1.6 W
5	Target distance	4.2 km/19.8 km
6	Sampling rate	250 MHz

applied in this field test is PointGrey-BFLY-PGE-13E4M-CS, whose pixel size is 5.3 μm and image size is 1280 pixels × 1024 pixels.

At the beginning of the field test, it is necessary to calibrate the relationship between the center of the emitted beam in coherent lidar and the image pixels of the visible light camera to attain the accurate pointing from coherent lidar to the distant target to be measured. Under the current experimental condition, pixel coordinates in the CCD corresponding to the emitted light beam are (368, 824).

After setting the above parameters, the target to be measured is selected from the test scenario. In this verification experiment, two physical targets in the scene shown in Fig. 7 were selected, respectively, and the approximate distances between the two targets and coherent lidar are 4.2 and 19.8 km, respectively, corresponding to the targets in the scenario one by one.

Manually rotate the servo aiming mechanism equipped with the transceiver telescope of the coherent lidar and the visible light camera, and point the pixel coordinates (368, 824) of the visible light-monitoring camera at the target to be measured located at 4.2 km in this experiment, as shown in Fig. 8. A digital acquisition device is applied to save long-pulse echo signals with coherent degradation, and then the echo signal is processed offline.

The same as the processing method in the above section, the proposed method in this paper is adopted to match the

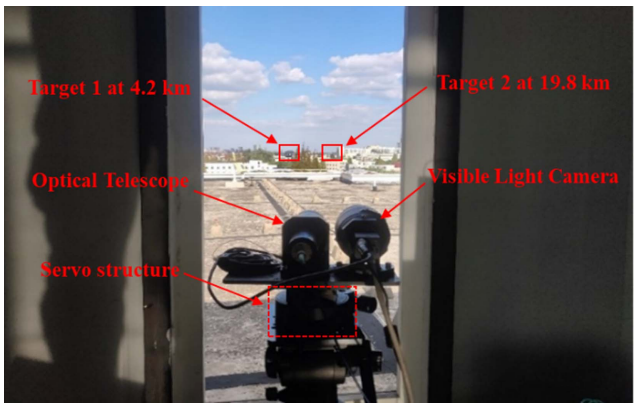

Fig. 7. Optical transceiver and target scenario in the field verification experiment.

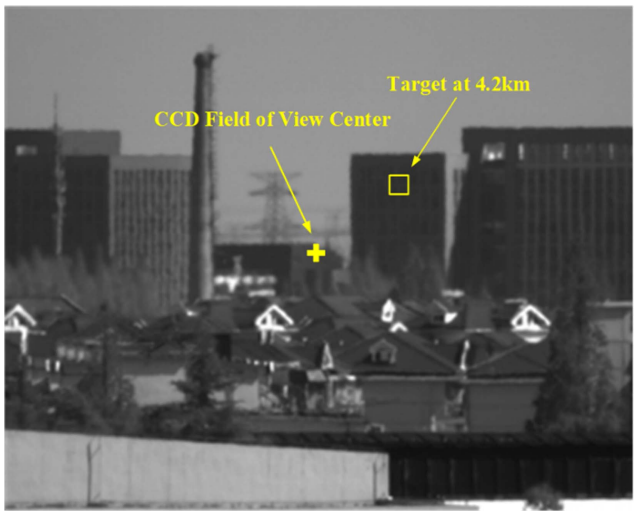

Fig. 8. Real target scenario at a distance of 4.2 km from the coherent lidar.

long-pulse echo signal after coherent degradation for a single pulse period using a random phase disturbance frequency of 500 Hz to 2.5 kHz; the processing results are obtained, as shown in Fig. 9(a). When the transmission optical power is 1.6 W and

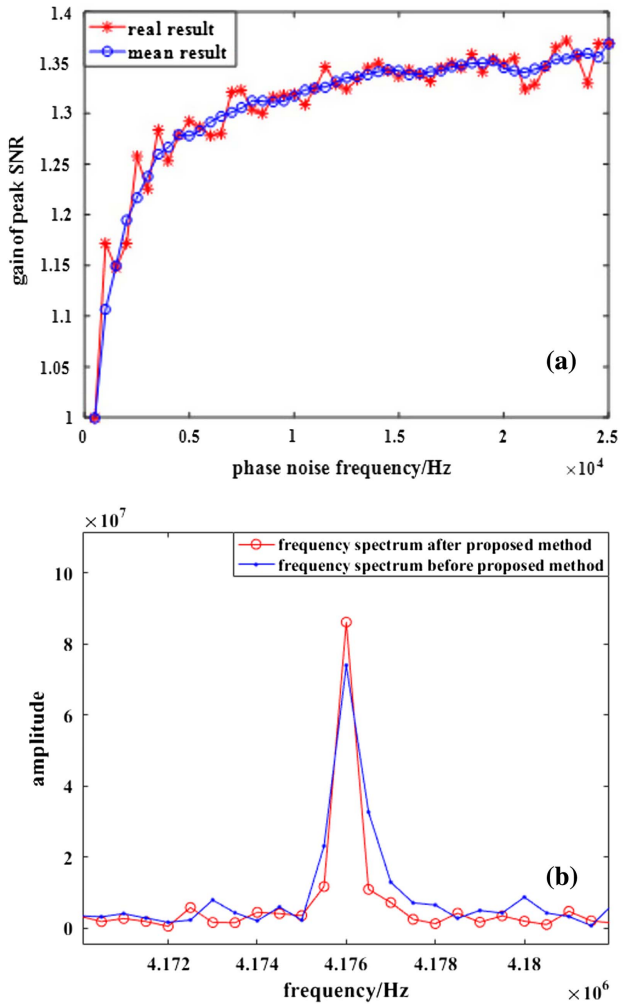

Fig. 9. Frequency spectrum and related results for the target at about 4.2 km. (a) Processing result of long-pulse echo signal with coherent degradation by the proposed method under different random phase-matching frequencies; (b) comparison of the frequency spectrum before and after being processed by this method.

the diameter of the transceiver telescope is 50 mm, for the target at 4.2 km, the long-pulse echo signal after coherent degradation in a single period has a certain initial SNR. The peak SNR gain of the long-pulse decoherence echo signal increases with the increasing frequency of the matching random phase disturbance. While the frequency of the random phase disturbance is 15 kHz, the uptrend of peak SNR gain becomes flat. At this time, the peak SNR of the long-pulse echo signal with coherent degradation suppression is increased by 0.35 times compared with the original long-pulse decoherence echo signal.

When a random phase disturbance frequency is 2.5 kHz and the iterative process reaches a convergence, Fig. 9(b) shows that the frequency spectral width of the long-pulse echo signal processed by this method is smaller than before.

To avoid the occasionality of echo signal processing results at 4.2 km, the pixel coordinates (368, 824) of the visible light-monitoring camera are aligned to the building target at 19.8 km. As shown in Fig. 10, the long-pulse decoherence echo signal is saved using a digital acquisition device, and then the echo signal is processed offline.

Similarly, the long-pulse coherence degradation signal is matched to a single pulse period with a random phase frequency of 500 Hz to 2.5 kHz using the intrapulse coherence degradation suppression method. The obtained processing results are shown in Fig. 11(a). Under the same condition, for the target at 19.8 km, the peak SNR gain of the long-pulse decoherence echo signal in a single pulse period increases and then remains relatively stable as the random phase-matching frequency gradually increases. When the matching frequency of random phase disturbance is 20 kHz, the rising trend of peak SNR gain becomes relatively flat. Comparing the long-pulse echo signal with intrapulse coherence degradation, the peak SNR of the long-pulse echo signal with coherence degradation suppression increases by about 4 times.

When a random phase disturbance frequency is 2.5 kHz and the iterative process reaches a convergence, Fig. 11(b) shows that the frequency spectral width of the long-pulse echo signal processed by this method is almost twice as small as before. In addition, the frequencies corresponding to the largest amplitude of the echo signal spectrum before and after being processed by this method are not the same; this shows that this method can result in the increasing range error as the SNR is decreasing.

Combined with the processing results of target echo signals at 4.2 and 19.8 km, it shows that during the process of target detection, the intrapulse coherence of long-pulse echo signals will indeed degrade due to the system hardware and external environment in coherent lidar. The method proposed in this paper can restore intrapulse coherence and improve the peak SNR to a certain extent. On the other hand, the target echo signal at different distances has different decoherence under the same condition. In general, the farther the target is from the coherent lidar, the more serious the intrapulse coherence degradation of its

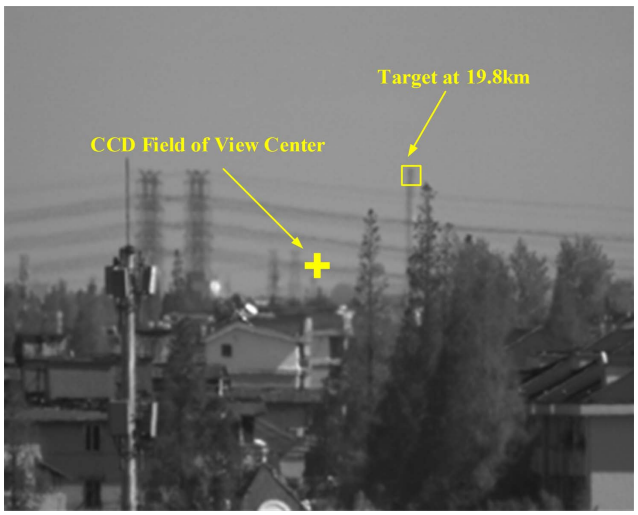

Fig. 10. Real target scenario at a distance of 19.8 km from the coherent lidar.

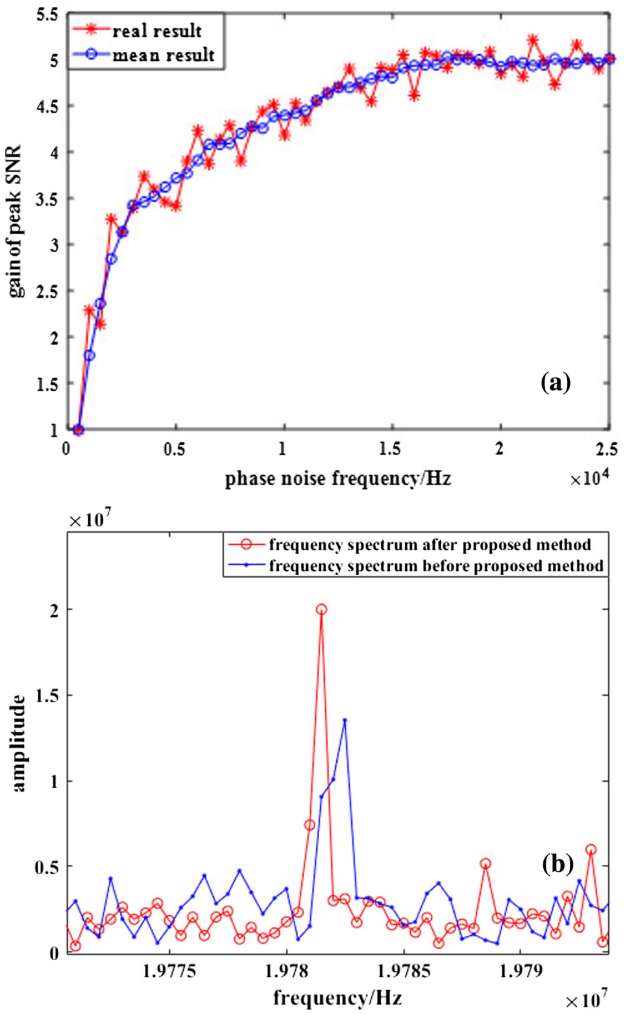

Fig. 11. Frequency spectrum and related results for the target at about 19.8 km. (a) Processing result of long-pulse echo signal with coherent degradation by the proposed method under different random phase-matching frequencies; (b) comparison of the frequency spectrum before and after being processed by this method.

echo signal will be. In this case, the coherence degradation suppression method proposed in this paper is more effective.

5. Conclusion

During target detection, long-pulse echo signal FMCW coherent lidar has the problem of intrapulse coherence degradation. As for this problem in long-pulse echo signals, first this paper gives a detailed theoretical analysis to demonstrate that coherence degradation can reduce the peak SNR of the echo signal, decreasing the detection probability of coherent lidar. And then a method to suppress the intrapulse coherence degradation of long-pulse echo signals is proposed to improve the target detection capability of coherent lidar.

This proposed method is verified from numerical simulations and field tests. These results show that the proposed method for suppressing intrapulse coherence degradation in the long-pulse echo signal can effectively suppress the coherent degradation of the echo signal, which is of great significance for coherent lidar in remote stationary target detection and weak signal detection. In future work, the specific reasons for coherence degradation in the long-pulse echo signal and the corresponding optimization methods will be further analyzed.

Acknowledgement

This work was supported by the National Key Research and Development Program of China (No. 2020YFB0408302) and the Strategic Priority Research Program of the Chinese Academy of Sciences (No. XDB43030400).

References

1. I. Kim, R. J. Martins, J. Jang, T. Badloe, S. Khadir, H.-Y. Jung, H. Kim, J. Kim, P. Genevet, and J. Rho, "Nanophotonics for light detection and ranging technology," Nat. Nanotechnol. **16**, 508 (2021).
2. T. Ogawa, H. Sakai, Y. Suzuki, K. Takagi, and K. Morikawa, "Pedestrian detection and tracking using in-vehicle lidar for automotive application," in *IEEE Intelligent Vehicles Symposium (IV)* (2011), p. 734.
3. M. Kutila, P. Pyykönen, H. Holzhüter, M. Colomb, and P. Duthon, "Automotive LiDAR performance verification in fog and rain," in *21st International Conference on Intelligent Transportation Systems (ITSC)* (2018), p. 1695.
4. D. J. Lum, "Ultrafast time-of-flight 3D LiDAR," Nat. Photonics **14**, 2 (2020).
5. A. J. Masino and C. Y. Young, "Atmospheric-induced frequency fluctuations in LIDAR," Proc. SPIE **5413**, 82 (2004).
6. D. G. Youmans and D. U. Fluckiger, "Linear FM chirp pulse compression ladar receiver operating characteristic: 'maximum of M Rayleighs' statistics," Proc. SPIE **3065**, 202 (1997).
7. E. Baumann, J. D. Deschênes, F. R. Giorgetta, W. C. Swann, I. Coddington, and N. R. Newbury, "Speckle phase noise in coherent laser ranging: fundamental precision limitations," Opt. Lett. **39**, 4776 (2014).
8. S. Kruse, M. Bahmanian, P. Kneuper, C. Kress, H. G. Kurz, T. Schneider, and J. C. Scheytt, "Phase noise investigation for a radar system with optical clock distribution," in *17th European Radar Conference (EuRAD)* (2021), p. 26.
9. M. Harris, G. N. Pearson, J. M. Vaughan, D. Letalick, and C. Karlsson, "The role of laser coherence length in continuous-wave coherent laser radar," J. Mod. Opt. **45**, 1567 (1998).
10. Q. Fu, Z. Zhou, Y. Luo, and S. Liu, "Laser distance measurement by triangular-wave amplitude modulation based on the least squares," Infrared Phys. Technol. **104**, 103146 (2020).
11. S. H. Lee, J. Lee, Y. J. Kim, K. Lee, and S.-W. Kim, "Active compensation of large dispersion of femtosecond pulses for precision laser ranging," Opt. Express **19**, 4002 (2011).
12. A. G. Luchinin, L. S. Dolin, and M. Y. Kirillin, "Time delay and width variation caused by temporal dispersion of a complex modulated signal in underwater lidar," Appl. Opt. **58**, 5074 (2019).
13. A. G. Luchinin, "Theory of underwater LIDAR with a complex modulated illumination beam," Izv. Atmos. Oceanic Phys. **48**, 663 (2012).
14. X. Fan, W. Jiaxing, Z. Daiyin, and T. Qi, "Speckle noise reduction technique for lidar echo signal based on self-adaptive pulse-matching independent component analysis," Opt. Lasers Eng. **103**, 92 (2018).
15. T. J. Karr, "Atmospheric phase error in coherent laser radar," IEEE Trans. Antennas Propag. **55**, 1122 (2007).
16. J. I. Davis, "Consideration of atmospheric turbulence in laser systems design," Appl. Opt. **5**, 139 (1966).
17. J. F. Holmes, J. S. Peacock, and D. C. Draper, "Optical remote sensing of surface roughness through the turbulent atmosphere," Appl. Opt. **33**, 7770 (1994).
18. X. Dong, Y. Hu, and S. Xu, "Analysis of coherent laser echo characteristics backscattered from rough Gaussian target," Optik **253**, 168512 (2022).

19. Z. Zheng, C. Zhao, H. Zhang, S. Yang, D. Zhang, H. Yang, and J. Liu, "Phase noise reduction by using a dual-frequency laser in coherent detection," Opt. Laser Technol. **80**, 169 (2016).
20. H. Zhao, B. Liu, G. Liu, F. Chen, Z. Zhuang, Y. Yu, and Y. Gan, "Nonlinearity correction and dispersion analysis in FMCW laser radar," Proc. SPIE **9297**, 929729 (2014).
21. R. Wang, B. Wang, M. Xiang, C. Li, S. Wang, and C. Song, "Simultaneous time-varying vibration and nonlinearity compensation for one-period triangular-FMCW lidar signal," Remote Sens. **13**, 1731 (2021).
22. T. Dilazaro and G. Nehmetallah, "Performance analysis of linearly-swept frequency-modulated continuous-wave ladar," Proc. SPIE **10925**, 173 (2019).
23. M. Yang, R. Cao, T. Li, B. Wu, P. Jiang, Y. Lu, and L. Jin, "Laser frequency sweep linearization by BP neural network for FMCW LiDAR," Proc. SPIE **11763**, 1176359 (2021).
24. X. Zhang, J. Pouls, and M. C. Wu, "Laser frequency sweep linearization by iterative learning pre-distortion for FMCW LiDAR," Opt. Express **27**, 9965 (2019).
25. Z. Yu, C. Lu, and G. Liu, "FMCW LiDAR with an FM nonlinear kernel function for dynamic-distance measurement," Opt. Express **30**, 19582 (2022).
26. S. Bai, X. Zhou, L. Zhang, H. Wang, and J. Yuan, "Nonlinear correction of frequency-modulated continuous-wave lidar frequency modulation based on singular value decomposition-least square algorithm," Opt. Eng. **59**, 056106 (2020).
27. Z. Xiao, Z. Wu, Z. Jiang, D. Yue, and G. Xia, "Experimental Investigation on the ranging resolution of a FMCW Lidar," Photonics **9**, 11 (2021).
28. J. Yang, B. Zhao, and B. Liu, "Long-range coherent lidar based on pulse-compression," Proc. SPIE **11763**, 117631E (2021).
29. P. Gallion and G. Debarge, "Quantum phase noise and field correlation in single frequency semiconductor laser systems," IEEE J. Quantum Electron. **20**, 343 (1984).